



# Macro-continuous dynamics for hyper-redundant robots: application to locomotion bio-inspired by elongated animals

Frédéric Boyer, Shaukat Ali, Mathieu Porez

## ► To cite this version:

Frédéric Boyer, Shaukat Ali, Mathieu Porez. Macro-continuous dynamics for hyper-redundant robots: application to locomotion bio-inspired by elongated animals. IEEE Transactions on Robotics, 2012, 28, pp.303 - 317. hal-00761258

**HAL Id: hal-00761258**

**<https://hal.science/hal-00761258>**

Submitted on 5 Dec 2012

**HAL** is a multi-disciplinary open access archive for the deposit and dissemination of scientific research documents, whether they are published or not. The documents may come from teaching and research institutions in France or abroad, or from public or private research centers.

L'archive ouverte pluridisciplinaire **HAL**, est destinée au dépôt et à la diffusion de documents scientifiques de niveau recherche, publiés ou non, émanant des établissements d'enseignement et de recherche français ou étrangers, des laboratoires publics ou privés.

# Macro-Continuous Dynamics For Hyper-Redundant Robots: Application to Kinematic Locomotion Bio-Inspired by Elongated body Animals

Frédéric Boyer, Shaukat Ali, and Mathieu Porez

**Abstract**—This article presents a unified dynamic modeling approach of (elongated body) continuum robots. The robot is modeled as a geometrically exact beam continuously actuated through an active strain law. Once included into the geometric mechanics of locomotion, the approach applies to any hyper-redundant or continuous robot devoted to manipulation and/or locomotion. Furthermore, exploiting the nature of the resulting model as being a continuous version of the Newton-Euler model of discrete robots, an algorithm is proposed which is capable of computing the internal control torques (and/or forces) as well as the rigid net motions of the robot. In general, this algorithm requires a model of the external forces (responsible for the self propulsion), but we will see how such a model can be replaced by a kinematic model of a combination of contacts related to terrestrial locomotion. Finally, in this case, that we name "kinematic locomotion", the algorithm is illustrated through many examples directly related to elongated body animals such as snakes, worms or caterpillars and their associated bio-mimetic artifacts.

**Index Terms**—Beam theory, bio-inspired locomotion, continuum robots, geometric mechanics, hyper-redundant robots, kinematic constraints, Newton-Euler dynamics.

## I. INTRODUCTION

Engineers have always been inspired by nature. In the beginning of robotics, robots resembling to human arm were designed using discrete mechanisms devoted to the manipulation tasks of industrial manufacturing processes. These discrete mechanisms consist of serial chains of rigid bodies connected by lumped degrees of freedom (DoFs) and are today included into the wider class of multibody systems. With the passage of time, the researchers in this field started developing mechanisms with more and more DoFs, thus introducing a new generation of robots called as hyper-redundant robots (HRRs) since they may be considered as having an infinite degree of redundancy with respect to the six dimensional task consisting of moving a rigid body in space. In case of locomotion, these systems are usually inspired by vertebrate elongated body animals such as snakes [1] and anguilliform fish [2], where the vertebrae correspond to the rigid bodies of the associated multibody system. From this point of view, these animals can be effectively considered as continuous, the

European eel having more than 130 vertebrae, while some species of big snakes have more than 500. Nowadays, thanks to the research on bio-mimetic robots, the concepts of continuum robots and soft-bodied robots are extending robotics even further. In fact, unlike traditional robots, these robots, inspired by the invertebrate organisms known as muscular-hydrostats, do not contain any rigid organs. Also, their shape changes are continuous along their body length similar to that of an elephant trunk [3], the mammalian tongue [4], caterpillars [5], earthworms [6], octopus arms [7] etc. Finally, all these systems today form the general class of continuous-like robots. Regarding their potential impact, let us first note that using the same single chain morphology, elongated body continuous like robots would offer a wide spectrum of applications ranging from manipulation to locomotion on earth as well as in water. Moreover, once connected to a discrete mechanism, they could be used as versatile manipulators as well as grippers. Finally, due to their slender morphology, they could play a crucial role to achieve rescue missions in unstructured, highly cluttered and confined environments e.g. collapsed buildings, narrow spaces etc.

With the progress of these researches, the extension of the basic robot models (geometric, kinematic and dynamic models) to these new systems became a crucial step towards their future success. Regarding this point, several researchers have done extensive work related to HRRs or continuous robots in order to investigate the usual problems of robotics such as motion planning, gait generation, kinematic and dynamic modeling, design and control etc. We refer the reader to [8] which surveys the state of the art on soft robotics. Historically, the initiative was undoubtedly taken by Hirose through his pioneering work related to the design and control of snake-like devices [1].

Based on these seminal works, many contributions to kinematic modeling have been proposed [3], [9]–[12]. Concerning dynamics of continuum robots, a few works on this topic have been proposed [13]–[16]. In fact, the existing approaches can be categorized into two main sets depending on whether the robot is considered as a multibody system with a large number of DoFs [17], [18], or directly as a continuous deformable medium. In the first case, the modeling is facilitated by the fact that mathematical tools from usual discrete robotics are already available. On the other hand, adopting a continuous model from the beginning can greatly facilitate the formulation, analysis and resolution of the robotics problems related to manipulation [15], [19] and locomotion [1], [10], [20].

Manuscript received Month Day, Year; revised Month Day, Year. The associate editor coordinating the review of this paper and approving it for publication was ...

The authors' are with the Ecole des Mines de Nantes, Nantes, France. (email: frederic.boyer@mines-nantes.fr, shaukat.ali@mines-nantes.fr, mathieu.porez@mines-nantes.fr)

Publisher Item Identifier .

However, applying this second type of approach necessitates giving a material reality to the continuum kinematics. For instance, the backbone curves of references [9], [10] have to be completed with a material lateral extension enabling the inertia of the robot to be defined as achieved in [15], [19] for planar robots. Alternatively, the Geometrically Exact Beam Theory (GEBT) of J.C. Simo [21], [22] has been used for the modeling of passive steerable needles in the context of medical robotics [23],[24], while in [8] and [25], it has been applied to the real soft robot OctArm [26]. In the GEBT, a beam is modeled as a one dimensional Cosserat medium [27], i.e. a multibody system made of an infinite number of rigid bodies, or cross sections, of infinitesimal length assembled along the line of their centroids, each cross section being able to move with respect to the others due to some strain time-variations.

Starting from this point of view, in [2] a continuous eel-like robot is modeled as a strain (curvature) - actuated geometrically exact beam. Pursuing a macroscopic modeling approach, each Cosserat cross section of the actuated beam mimics a vertebra of the animal (here the eel), while the imposed strain law models the actuated infinitesimal joints of the corresponding continuous rigid robot. Once related to the general theory of locomotion on principal fiber bundles [28], such a model can be used to solve the following two problems both using the curvature time law as control input: 1) compute the control internal torques (and/or forces), i.e. solve the inverse torque dynamics. 2) compute the net motion of a reference cross section (for instance attached to the head) propelled by the external forces exerted by the surroundings (i.e., solve the forward locomotion dynamics). The approach was termed macro-continuous since, like the Variable Geometry Truss evoked in [19], it is suitable for modeling hyper-redundant robots at a macroscopic scale where they can be approximated as a beam. It is naturally adapted to the highest levels of the mechanical design as well as the generation of complex gaits involving a lot of DoFs as this is usually the case of HRRs [20].

In the article here presented, we reconsider this approach for locomotion and extend it to cases where: 1) The configuration space of the cross sections is an arbitrary Lie group. 2) The control strain law is arbitrary (curvature, twist, stretching...). 3) The external forces responsible for the propulsion are not forced to be those produced by a fluid but can be imposed by the contact with the ground and modeled through kinematic constraints.

In this case, like discrete multibody systems [29], when the number of independent constraints is larger than the number of net motions DoFs, the locomotion dynamics are replaced by a kinematic model entirely governed by the constraints. Geometrically, these forward locomotion kinematics are nothing but a continuous version of the finite-dimensional kinematic connections of nonholonomic mechanics [28], [30]. As a consequence and contrary to the case of eel swimming, the locomotion dynamics are not required to deduce the net motions but are used in their inverse form to compute the resultant and moment of external forces produced by the contacts. Once these elements are computed, they are distributed on the contacts in order to fix a possible set of external reaction

forces and couples which are used in a second step by the algorithm to compute the internal actuation torques and/or forces. Finally, the kinematic constraints are deduced from the model of a few types of contacts, which will allow us to apply the macro-continuous approach to terrestrial locomotion of several elongated body animals as earthworms (crawling worm), inchworms (measuring caterpillars), snakes in planar and three-dimensional lateral undulations.

This article is structured as follows. In section II, we take an in-depth look at the parametrization of GEBT particularly, the strain field definitions and their relation to discrete joint kinematics. Section III presents a comparative study of the beam kinematics and HRRs. Based upon the parametrization of section II, the continuous kinematic and dynamic models are stated in section IV. In section V, the continuous Newton-Euler computed-torque algorithm of [2] is presented in a more general context. In section VI, the common types of terrestrial contacts are modeled as kinematic constraints. Based upon the model of contact, a modified algorithm is developed in section VII. Finally, in section VIII the proposed approach is illustrated by examples related to terrestrial locomotion robots bio-inspired by elongated body animals.

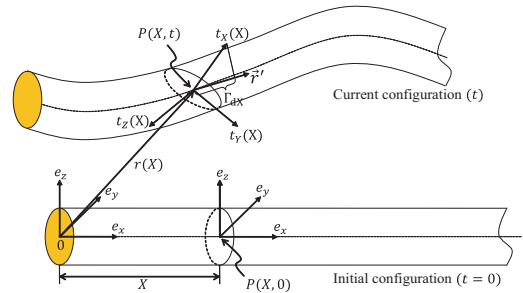


Fig. 1. Frames and parametrization

## II. BASIC NOTATIONS AND DEFINITIONS

In the subsequent sections, we use the language of geometric mechanics [31] as this has already been adopted by [2], [23], [32] in the context of continuum robots. In this regard,  $G \subseteq SE(3)$  is a  $n$  dimensional Lie group of transformations of the ambient space provided with an orthonormal fixed frame  $\mathcal{F}_s = (O, e_x, e_y, e_z)$ . The Lie algebra of  $G$  is denoted by  $\mathfrak{g}$  and defined as the space of infinitesimal transformations or twists, i.e. the tangent space to  $G$  at  $g = 1$  endowed with the Lie bracket  $[\cdot, \cdot]$ . Introducing the internal product on  $\mathfrak{g}$ , we define  $\mathfrak{g}^*$ , the vector space of 1 forms on  $\mathfrak{g}$ , or wrenches. Differentiating the group automorphism  $h \in G \mapsto ghg^{-1}$  at  $h = 1$ , gives the action map  $Ad_g$  of  $G$  on  $\mathfrak{g}$ . Then differentiating  $Ad_g$  with respect to  $g$  at  $g = 1$  defines the adjoint map  $ad_{(\cdot)}$  of  $\mathfrak{g}$  on  $\mathfrak{g}$ . Dualizing  $ad_{(\cdot)}$  defines the co-adjoint map of  $\mathfrak{g}$  on  $\mathfrak{g}^*$  while  $Ad_{(\cdot)}^*$  is the co-action of  $G$  on  $\mathfrak{g}^*$ . See Appendix A for more usual definition of these operators as well as their matrix expressions in  $SE(3)$ .

For any vector  $V \in \mathbb{R}^3$ ,  $V^\wedge$  (or  $\hat{V}$ ) denotes the cross-product matrix of  $V$  while if  $V = (v^T, \omega^T)^T \in \mathbb{R}^6$ , then

$V^\wedge = \begin{pmatrix} \hat{\omega} & v \\ 0 & 0 \end{pmatrix}$ , where  $\omega \in \mathbb{R}^3$  and  $(\hat{V})^\vee = V$ . In agreement with [2], a hyper-redundant robot may be modeled by a Cosserat beam in finite 3D transformations and small strains with the backbone curve of the robot assimilated to the beam centroidal line. In this approach, each cross section of the beam (of length  $l$ ), supposed rigid, is labeled by its abscissa  $X$  in the initial configuration in which the beam is straight and aligned on  $(O, e_x)$  (see Fig. 1). At any rigid cross section  $X$ , a mobile orthonormal frame is attached  $t \mapsto \mathcal{F}_m(X, t) = (P, t_X, t_Y, t_Z)(X, t)$  whose origin  $P(X)$  and the first vector  $t_X(X)$  coincide with the center of the cross section and its unit normal vector, respectively. With this choice, the configuration of any mobile frame is defined by the action of an element of  $g \in SE(3)$  applied to the fixed frame  $\mathcal{F}_s$ . It thus becomes possible to introduce the first definition of the robot configuration space as a functional space of curves in  $SE(3)$ , parameterized by the material abscissa, i.e.:

$$\mathcal{C}_1 = \{g : \forall X \in [0, l] \mapsto g(X) \in SE(3)\}. \quad (1)$$

Later, we will introduce a second definition of configuration space as a principal fiber bundle. The derivative operators  $\partial(\cdot)/\partial X$  and  $\partial(\cdot)/\partial t$  will be indicated as a "prime" and a "dot", respectively. On the robot, two vector fields are defined in  $se(3)$ . The first is the time-twist field:

$$\hat{\eta} : X \in [0, l] \mapsto \hat{\eta}(X, t) = g^{-1}\dot{g} \in se(3), \quad (2)$$

where  $\eta(X, t)$  defines the infinitesimal transformation undergone by the cross section  $X$  between two infinitely close instants  $t$  and  $t + dt$ . The second is the space-twist field such that:

$$\hat{\xi} : X \in [0, l] \mapsto \hat{\xi}(X, t) = g^{-1}g' \in se(3), \quad (3)$$

where  $\xi(X, t)$  defines the infinitesimal transformation undergone by the cross section  $X$  at fixed time  $t$  when the material axis slides from  $X$  to  $X + dX$ . Now depending on the considered robot, certain degrees of freedom between any two contiguous cross sections are actuated while others are constrained to constant values through the design of internal joints (that are assumed ideal). Mathematically, this corresponds to identify  $\hat{\xi}$  to a desired control field explicitly dependent on the time and noted  $\hat{\xi}_d(t)$ , i.e.:

$$\xi(X) = \xi_d(X, t), \forall (X, t) \in [0, l] \times \mathbb{R}^+. \quad (4)$$

Finally,  $\xi_d$  parameterizes the internal kinematics of the robot, i.e. the continuous infinitesimal homologous of the usual internal joints of discrete multibody systems.

### III. BEAM-KINEMATICS AND HRRS

We now list the different possible actuations of  $\xi$  and comment their relations to continuum robotics and beam theory. For this, we start from definition (4) which we detail as follows:

$$g^{-1}g' = \begin{pmatrix} R^T R' & R^T r' \\ 0 & 0 \end{pmatrix} = \begin{pmatrix} \hat{K}_d(t) & \Gamma_d(t) \\ 0 & 0 \end{pmatrix} = \hat{\xi}_d(t), \quad (5)$$

where  $K_d = (K_{dX}, K_{dY}, K_{dZ})$  and  $\Gamma_d = (\Gamma_{dX}, \Gamma_{dY}, \Gamma_{dZ})$ . The components of these two vectors have the following

meanings:  $K_{dX}$  is the rate of twist per unit of material beam length while  $K_{dY}$  and  $K_{dZ}$  represent the curvatures of its centroidal line in the planes  $(P, t_X, t_Z)$  and  $(P, t_X, t_Y)$  respectively. In the same way,  $\Gamma_{dX} - 1$  is the rate of stretching of the centroidal line (see Fig. 1) while  $\Gamma_{dY}$  and  $\Gamma_{dZ}$  are the local transverse shearing rotations around the axes  $(P, t_Z)$  and  $(P, t_Y)$  respectively. Now, depending on whether these scalar strain fields are actuated or not, different cases, relevant to robotics, are possible, from that where the internal kinematics are the most actuated to where they are the least actuated as summarized in table I:

TABLE I  
ACTUATED DOFS VS BEAM THEORY

Case	Constraints	DoFs	Beam Theory	Remarks
1	No constraints	06	Timoshenko-Reissner	Full actuated beam
2	$\Gamma_{dY} = \Gamma_{dZ} = 0$	04	Extensible Kirchhoff	Cross sections stay perpendicular to vertebral axis
3	Case 2 with $\Gamma_{dX} = 1$	03	Inextensible Kirchhoff	infinitesimal version of a spherical joint
4	Case 3 with $K_{dX} = 0$	02	No corresponding beam	In passive beams, 3D bending always produce torsion
5	Case 4 with $K_{dY} = 0$	01	Inextensible planar Kirchhoff	Planar case with Yaw DoF actuation

#### Remarks:

- Each of these internal DoFs finds an application in nature for elongated body animals' locomotion. In fact, one of the two curvatures  $K_Y$  and  $K_Z$  actuates the yaw in the plane of propulsion, while the other actuates the pitch for complex 3D maneuvers involving the body. The torsion  $K_X$  has a direct action on the roll whose control is crucial to stabilize the orientation of the head of robots bio-inspired by eels for instance. As for linear DoFs,  $\Gamma_X$  actuates the traction-compression as used by large snakes while  $\Gamma_Y$  and  $\Gamma_Z$  can be actuated through the movements of the skin and scales with respect to the backbone.
- A similar relation to (5) exists in the case of any subgroup of  $SE(3)$ . Also, in the following, we will consider (5) with  $g$  belonging to any subgroup  $G$  of  $SE(3)$  of Lie algebra  $\mathfrak{g}$ .

### IV. THE CONTINUOUS MODEL OF HRRS

From now on,  $g_o$ ,  $\dot{g}_o$  and  $\ddot{g}_o$  denote the position, velocity and acceleration of the cross section  $X = 0$  on  $G$ , respectively. The continuous dynamic model of a HRR splits into 5 sub-models detailed in the following subsections.

#### A. Continuous model of transformations

This is immediately derived from definition (5) of internal DoFs:

$$g' = g\hat{\xi}_d(t), \quad (6)$$

with boundary conditions:  $g(X = 0) = g_o$ .

### B. Continuous model of velocities

By taking derivative of (2) with respect to space (i.e.  $X$ ), and by invoking (5), we obtain:

$$\eta' = -ad_{\xi_d(t)}(\eta) + \dot{\xi}_d(t), \quad (7)$$

with boundary conditions:  $\eta(X=0) = \eta_o = (g_o^{-1}\dot{g}_o)^\vee$ .

### C. Continuous model of accelerations

This is inferred by taking derivative of the previous model (7) with respect to time:

$$\eta' = -ad_{\xi_d(t)}(\dot{\eta}) - ad_{\dot{\xi}_d(t)}(\eta) + \ddot{\xi}_d(t), \quad (8)$$

whose solutions are fixed by the boundary conditions:  $\dot{\eta}(X=0) = \dot{\eta}_o = (g_o^{-1}\ddot{g}_o - g_o^{-1}\dot{g}_o g_o^{-1}\dot{g}_o)^\vee$ .

*Remark 3:* On reconsidering the continuous kinematic model (6), it becomes clear that it is always possible to reconstruct the configuration of the beam from the knowledge of  $g_o$  and that of the strain field  $\xi_d$ . Thus, a second definition of the configuration space of a robot can be given as the principal fiber bundle:

$$\mathcal{C}_2 = G \times \mathcal{S}, \quad (9)$$

where  $G$  stands for the configuration of the head frame, while  $\mathcal{S}$  is the shape space here defined as the following functional space of curves in the Lie algebra:

$$\mathcal{S} = \{\xi : \forall X \in [0, l] \mapsto \xi(X) \in \mathfrak{g}\}. \quad (10)$$

In this second definition of the robot configuration space, the cross section  $X=0$  plays the role of reference body, i.e. a body whose motion defines the reference of rigid overall motions with respect to which the shape deformations are measured. In bio-mimetics, this reference body is usually attached to the head of the bio-inspired robot.

### D. Dynamics on $\mathcal{C}_1$ : continuous model of the internal torques

By applying on  $\mathcal{C}_1$  the Hamilton principle for a continuum robot subject to a density of imposed external wrenches per unit of beam length  $\overline{F}$  on  $]0, l[$  and two punctual external wrenches  $F_-$  and  $F_+$  imposed on  $X=0$  and  $X=l$  respectively, one obtains the following Partial Differential Equations (PDE) [33]:

$$\frac{\partial}{\partial t} \left( \frac{\partial \mathcal{L}}{\partial \eta} \right) - ad_\eta^* \left( \frac{\partial \mathcal{L}}{\partial \eta} \right) + \frac{\partial}{\partial X} \left( \frac{\partial \mathcal{L}}{\partial \xi} \right) - ad_\xi^* \left( \frac{\partial \mathcal{L}}{\partial \xi} \right) = \overline{F}, \quad (11)$$

whose solutions are fixed at each instant by the boundary conditions:

$$\frac{\partial \mathcal{L}}{\partial \xi}(0) = -F_- \text{ , and: } \frac{\partial \mathcal{L}}{\partial \xi}(l) = F_+, \quad (12)$$

where the Lagrangian density of a continuum robot has been defined by  $\mathcal{L} = \mathfrak{T} - \mathcal{U} = (1/2)(\eta^T(\mathcal{M}\eta) - \Lambda^T(\xi - \xi_d(t)))$ , with:  $\mathcal{M} \in \mathfrak{g}^* \otimes \mathfrak{g}$ , the inertia tensor density, and  $\partial \mathcal{U} / \partial \xi = \Lambda \in \mathfrak{g}^*$ , the density of internal wrenches ensuring the forcing of the Lagrangian internal kinematic constraints:  $\xi = \xi_d(t)$ . Let us note here that  $\Lambda$  is a field of Lagrange multipliers and that, for the actuated internal DoFs, the associated multipliers are forces

or/and torques exerted by the actuators while for the passive DoFs, the multipliers are internal reaction torques or forces. Note also that with such a choice, the internal kinematics are assumed to be inelastic and the robot turns out to be a continuous rigid robot<sup>1</sup>. Now, if we note  $\partial \mathfrak{T} / \partial \eta = \mathcal{M}\eta$  the density of kinetic wrench along the robot, we find:

$$\mathcal{M}\dot{\eta} - ad_\eta^*(\mathcal{M}\eta) - \Lambda' + ad_{\xi_d(t)}^*(\Lambda) = \overline{F}, \quad (13)$$

with boundary conditions:

$$\text{at } X=0: \Lambda(0) = -F_- \text{ and at } X=l: \Lambda(l) = F_+. \quad (14)$$

Finally, (13) and (14) are considered in the following as the dynamics of the internal wrenches or more simply as the "internal dynamics".

### E. Dynamics on $\mathcal{C}_2$ : dynamics of the reference body

The dynamics on  $\mathcal{C}_2$  are derived from those on  $\mathcal{C}_1$  by forcing the virtual and real velocity fields in the Hamilton principle (which previously led to (13-14)) to verify the following constraint:

$$\eta = Ad_k(\eta_o), \quad (15)$$

where,  $k = g^{-1}g_o$ . Note that, the defined field (15) is simply the time-twist field on the beam induced by the movement of the head alone, while the body is frozen in its current shape. In these conditions, the internal wrenches do not work in such a field and the balance of virtual work reduces to:

$$\int_0^l Ad_k^*(\mathcal{M}\dot{\eta} - ad_\eta^*(\mathcal{M}\eta) - \overline{F})dX = Ad_{k+}^*F_+ - F_-, \quad (16)$$

where  $\dot{\eta}$  is replaced by the acceleration field compatible with (15), i.e.:

$$\begin{aligned} \dot{\eta} &= Ad_k(\dot{\eta}_o) + ad_\eta(Ad_k(\eta_o)) + Ad_k(\eta_o^2) - (Ad_k(\eta_o))^2 \\ &= Ad_k(\dot{\eta}_o) + \zeta, \end{aligned} \quad (17)$$

which defines  $\zeta(X)$  as the material (or body) acceleration of cross section  $X$  induced by the body shape motion and the movement of the head except for its pure acceleration (i.e.  $\dot{\eta}_o$ ).

Finally, when the calculations are done and the kinematic reconstruction equation  $\dot{g}_o = g_o\dot{\eta}_o$  is taken into account, the dynamic equations on  $\mathcal{C}_2$  can be written as:

$$\begin{pmatrix} \dot{\eta}_o \\ \dot{g}_o \end{pmatrix} = \begin{pmatrix} \mathcal{M}_o^{-1}(\xi_d)F_o(\xi_d, \dot{\xi}_d, \ddot{\xi}_d, g_o, \eta_o) \\ g_o\dot{\eta}_o \end{pmatrix}, \quad (18)$$

with:  $F_o = F_{in} + F_{ext}$ , and where we introduced the inertia tensor of the whole robot reduced to the reference cross section i.e. in  $X=0$ :

$$\mathcal{M}_o = \int_0^l Ad_k^* \mathcal{M} Ad_k dX, \quad (19)$$

as well as the external wrenches, reduced to the reference cross section:

$$F_{ext} = -F_- + Ad_{k+}^*F_+ + \int_0^l Ad_k^*(\overline{F})dX, \quad (20)$$

<sup>1</sup>Alternatively, the model of internal dynamics can be enriched by adding elastic and viscous terms in  $\mathcal{U}$

and the inertial wrenches reduced to the reference cross section:

$$F_{in} = - \int_0^l Ad_k^*(\mathcal{M}\zeta - ad_\eta^*(\mathcal{M}\eta))dX. \quad (21)$$

In the following, (18) will be considered as the dynamics of the reference body net motions controlled by the shape time variations, i.e. the "locomotion dynamics".

## V. DYNAMIC ALGORITHM OF THE CONTINUUM ROBOTS

By defining the kinematic state vector  $\mathcal{X}_1 = (g, \eta, \dot{\eta})$ , the kinematic models (6,7,8) can be easily grouped together into a single spatial Ordinary Differential Equation (ODE):

$$\mathcal{X}'_1 = f_1(\mathcal{X}_1, \xi_d(t), \dot{\xi}_d(t), \ddot{\xi}_d(t)). \quad (22)$$

Similarly, the internal dynamics (13) can be stated in the form of the following spatial ODE, of the state vector  $\mathcal{X}_2 = (\mathcal{X}_1, \Lambda)$ :

$$\mathcal{X}'_2 = f_2(\mathcal{X}_2, \xi_d(t), \dot{\xi}_d(t), \ddot{\xi}_d(t)), \quad (23)$$

$$\text{with: } f_2 = \begin{pmatrix} f_1 \\ ad_{\xi_d(t)}^*(\Lambda) + \mathcal{M}\dot{\eta} - ad_\eta^*(\mathcal{M}\eta) - \overline{F} \end{pmatrix}. \quad (24)$$

Then, the terms appearing in the locomotion dynamics (18) can also be calculated by spatial integration of a single ODE of the state vector  $\mathcal{X}_3 = (\mathcal{X}_1, \mathcal{M}_o, F_o)$ :

$$\mathcal{X}'_3 = f_3(\mathcal{X}_3, \xi_d(t), \dot{\xi}_d(t), \ddot{\xi}_d(t)), \quad (25)$$

$$\text{with: } f_3 = \begin{pmatrix} f_1 \\ Ad_k^* \mathcal{M} Ad_k \\ Ad_k^*(ad_\eta^*(\mathcal{M}\eta) + \overline{F} - \mathcal{M}\dot{\eta}) \end{pmatrix}, \quad (26)$$

where the  $\zeta$  of (21) can be replaced by  $\dot{\eta}$  in (26) if the initial spatial conditions of (25) verify  $\dot{\eta}(X=0) = \dot{\eta}_o = 0$ . In fact, in this case (17) shows that  $\zeta = \dot{\eta}$  all along the beam. Finally, as we will now see, in every case the algorithm integrates (25) in these conditions, so that (26) makes sense.

All the above ODEs form a general algorithm as shown in

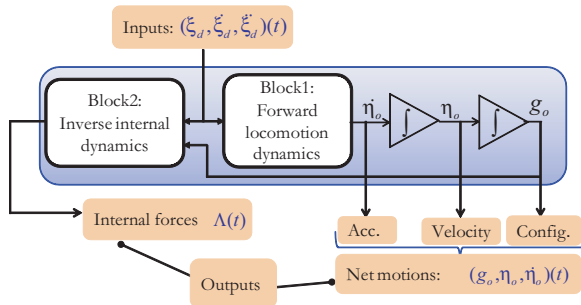


Fig. 2. General algorithm of HRRs

Fig. 2 to solve the dynamics of a HRR. The execution of algorithm is summarized as follows:

- 1) In block 1, integrate the spatial ODE (25) from  $X = 0$  to  $X = l$  initialized by  $\mathcal{X}_3(0) = (g_o, \eta_o, 0, 0, F_-)$ , to give  $\mathcal{M}_o$  and  $F_o$ .

- 2) In block 1, calculate  $\dot{\eta}_o$  and then integrate (18) between  $t$  and  $t + \Delta t$  in order to deduce the new reference state (for the following time-step):  $(g_o, \eta_o)(t + \Delta t)$
- 3) In block 2, integrate the spatial ODE (23) from  $X = 0$  to  $X = l$  initialized by  $\mathcal{X}_2(0) = (g_o, \eta_o, \dot{\eta}_o, F_-)$  to give  $\Lambda$  (and  $F_+$  by way of verification).

Remarks:

- Let us remark that the above algorithm is nothing else but a continuous version of the Newton-Euler discrete algorithm of mobile multibody systems of [29], where (22) stands for the forward recursive kinematics, (23), for the backward recursive computation of inter-body wrenches, and (25) stands for the recursive computation of the locomotion dynamics.
- The algorithm solves the forward dynamics by computing the net (reference) acceleration from a model of the external forces. In general, such a model can be very complex as in the case of swimming in which, in the absolute, it requires to integrate the Navier-Stokes equations of the surrounding flow [34]. In the case of terrestrial locomotion, the above algorithm can be used with external forces modeled as physical laws, e.g. friction laws. However, for the sake of simplicity of analysis, it can be useful to consider the contacts as ideal. In this case, they can be modeled as constraints instead of forces as discussed in the following section. In the next step, we will see that when the number of constraints is sufficient, locomotion dynamics can be replaced by kinematics and the locomotion is named as "kinematic locomotion".

## VI. KINEMATIC MODELING OF CONTACTS

In this work, we consider two types of contacts: anchorages and supports. Anchorages are modeled as bilateral holonomic constraints while supports are modeled as non-holonomic constraints. In both cases the contacts are distributed along the body axis. In the case of anchorages, two types are envisaged: either the anchorage is fixed on the material axis of the robot on an abscissa, noted  $C$ , constant in relation to time or, in contrast, this abscissa, noted  $C(t)$ , is explicitly dependent on time. The former is known as a locked anchorage and the latter is a sweeping anchorage. Concerning supports, the contact is always sweeping, as the robot can slide freely thanks to an annular type contact (see Fig. 3). Anchorages and supports are assumed to be attached to rigid bodies submitted to imposed relative motions in the fixed earth frame. Finally, as we will

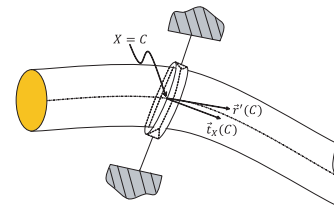


Fig. 3. Annular contact (CSFS)

see when considering examples, these models are of great

practical interest for modeling numerous locomotion modes as illustrated in table II.

TABLE II  
CONTACTS IN TERRESTRIAL LOCOMOTION

Type	Constraint	Locomotion	Examples
Locked anchorage	Clamped to earth	Step by step locomotion	Inchworm
Sweeping anchorage	Rolling without slipping	Axial propulsion	Earthworm, big snakes
Support	Non-sliding	Lateral undulation	Snakes

### A. Anchorages

For a locked anchorage as shown in Fig. 4(a), where the robot is anchored at a fixed material point  $C \in [0, l]$ , we write the geometric model as:

$$g(C) = g_c(t), \quad (27)$$

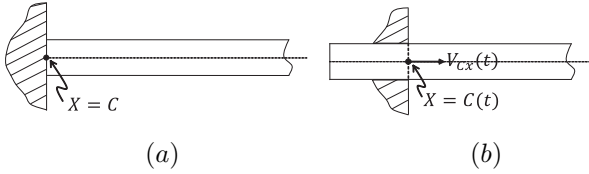


Fig. 4. (a) Locked anchorage; (b) Sweeping anchorage

where  $t \mapsto g_c(t)$  denotes a function of time in  $G$  which represents the imposed motion of the anchored rigid body. In particular, if  $g_c$  is independent of time, then this body is fixed, as in the case of a manipulator robot anchored in the ground or more simply a cantilevered beam (see Fig. 4(a)). For a sweeping anchorage as shown in Fig. 4(b)), the geometric model of contact cannot distinguish it from a locked anchorage, both considered at the same instant  $t$ . In fact, in the second case, we still have:

$$g(C(t)) = g_c(t), \quad (28)$$

which coincides with (27) when  $C = C(t)$ . In contrast, the kinematic model can make the distinction since, for the sweeping anchorage, by taking total derivative with respect to time (denoted as  $d(\cdot)/dt$ ) of (28):

$$\frac{d}{dt}g(C(t)) = \dot{g}(C(t)) + g'(C(t))\dot{C}(t) = \dot{g}_c(t), \quad (29)$$

which is multiplied by  $g^{-1}(C(t))$  to obtain, invoking (28) again, the sweeping anchorage constraints in  $\mathfrak{g}$ :

$$\eta(C(t)) + \xi_d(C(t), t)\dot{C}(t) = \eta_c(t), \quad (30)$$

where  $\eta_c(t) = (g_c^{-1}\dot{g}_c)^\vee(t)$ ,  $(\eta_c(t) = (V_{cX}, V_{cY}, V_{cZ}, \Omega_{cX}, \Omega_{cY}, \Omega_{cZ})^T(t)$ , when  $G = SE(3)$ ) is the time-twist imposed on the rigid body supporting the anchorage and where (30) allows one to recover the kinematic form of a locked anchorage:  $\eta(C) = \eta_c(t)$  when  $C$  is time-independent. Finally, let us note that (30) produces a set of  $\dim(\mathfrak{g})$  independent scalar constraints.

### B. Supports

Before describing the details of their modeling, let us recall that supports are sweeping by nature so they can only be accounted for by kinematic constraints. Here, we consider supports named as Cross Sectional Follower Supports (CSFS). Such supports follow the cross sections in their lateral motions (see Fig. 3). A CSFS is an annular joint preventing all relative translation velocities (of the beam with respect to the support) in the plane of a given cross section of abscissa  $X = C$ . Thus, for a movement in the space  $\mathbb{R}^3$  (i.e.  $G = SE(3)$ ), such a contact exerted in any  $C \in [0, l]$  is modeled by the relations:

$$(\dot{r}(C) - \dot{r}_c(t)) \times t_X(C) = 0, \quad (\omega(C) - \omega_c(t))^T t_X(C) = 0 \quad (31)$$

where  $\omega(X) = (\dot{R}R^T)^\vee(X)$  denotes the spatial angular velocity of the  $X$ -cross-section while  $(\dot{r}_c^T, \omega_c^T)^T(t)$  is the spatial twist imposed on the rigid support. After computation, (31) leads to the following three non-holonomic constraints

$$V_Y(C) = V_{cY}(t), \quad V_Z(C) = V_{cZ}(t), \quad \Omega_X(C) = \Omega_{cX}(t), \quad (32)$$

where  $V_{cY}(t), V_{cZ}(t)$  are the lateral velocities expressed in the cross section frame while  $\Omega_{cX}(t)$  is the axial component of the angular velocities. All of them being imposed on the  $C$ -cross-section by the movement of the obstacle, these velocities are null if the obstacle in question is fixed. Finally,  $C$  can itself move along the material robot axis following a time law of the general form:

$$\dot{C} = V_{cX}(t) - V_X(C), \quad (33)$$

where  $V_{cX}$  is imposed by the axial motion of the support while  $V_X(C)$  is ruled by the locomotion. Lastly, let us note that when the given support follows the cross section not only laterally but also axially, then  $\dot{C} = V_{cX}(t) - V_X(C) = 0$ .

### C. Models of contact forces

As the contacts are ideal, the reaction (contact) forces are identified as Lagrange multipliers associated to the scalar constraints taken from (30) and (32). When  $G = SE(3)$ , an anchorage introduces six multipliers (i.e. the six components of a complete reaction wrench) while a support transmits two lateral forces and one axial torque for a three-dimensional movement and only one lateral force for a planar motion. When the anchorages and/or the supports are imposed at the ends, the reaction forces associated with them enter into the calculation of the dynamics via a contact component of the apical external wrenches  $F_\pm$  that we note  $F_{c,\pm}$  (where "c" means "contact"). As long as the contacts are defined inside the domain of the beam, i.e. if  $C \in ]0, l[$ , then each of them adds a set of kinematic constraints in  $\mathfrak{g}$  and an associated reaction wrench (defined in  $\mathfrak{g}^*$ ), that enters into the model via  $\bar{F}$  which then contains a contact term of the form:  $\bar{F}_c(C)\delta(X - C)$ , where  $\delta$  denotes the Dirac distribution. Finally, according to (20), any distribution of contacts produces a contribution to  $F_{ext}$  which is noted  $F_c$  and called the resultant of the reaction (contact) wrenches.



## VII. ALGORITHM IN KINEMATIC CASE

When the number of constraints (imposed by the contacts) is equal or higher than the dimension of the fiber of  $\mathcal{C}_2$ , the system is said fully or over constrained and the net motions are entirely ruled by the kinematic model of the contacts which takes the most general explicit form:

$$\dot{g}_o = g_o \dot{\eta}_o = g_o \hat{f}(g_o, \xi_d(t), \xi_d'(t), \xi_d''(t), \dots, \xi_d(t)), \quad (34)$$

where the model of reference accelerations can be obtained by simple time differentiation of  $f$ . In this case, the locomotion is called "kinematic locomotion" (to distinguish it from the previous dynamic locomotion case) and the locomotion dynamics (18) are used in their inverse form to calculate the contact wrench induced by the external constraints, i.e.:

$$F_c = \mathcal{M}_o \dot{\eta}_o - F_{in} - F_{other}, \quad (35)$$

where  $F_{other}$ , denotes the contribution to  $F_{ext}$  brought by the distribution of external forces of other origin than contact. Such a distribution will be denoted by  $(F_{other,\pm}, \bar{F}_{other})$  and models external loads as gravity, pressure and viscous forces etc.

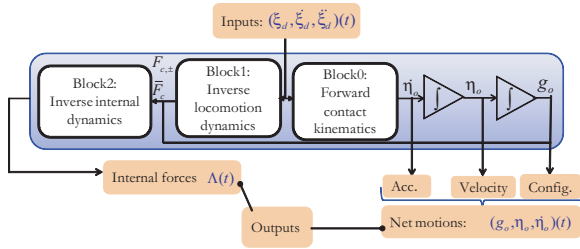


Fig. 5. Algorithm of a HRR with kinematic constraint model

Going further, when the number of constraints is strictly higher than the dimension of the fiber of  $\mathcal{C}_2$ , the overall motions of the robot are over-constrained which means that: 1) the internal movements must be compatible<sup>2</sup>, 2) the reaction unknowns  $F_{c,\pm}$  and  $\bar{F}_c$  are under-determined as they are only required to verify the locomotion dynamics (35). Finally, taking these considerations into account, the new constrained algorithm as shown in Fig. 5 can be summarized as follows:

- 1) In Block0, calculate  $(\eta_o, \dot{\eta}_o)$  from a kinematic model of contacts of the form (34) and its time derivative, and integrate  $\eta_o$  between  $t$  and  $t + \Delta t$  in order to deduce the new configuration of the reference cross section (for the following time-step):  $g_o(t + \Delta t)$ .
- 2) In Block1, integrate the spatial ODE (25) from  $X = 0$  to  $X = l$  initialized by  $\mathcal{X}_3(0) = (g_o, \eta_o, 0, 0, F_{other,-})$  and with  $\bar{F} = \bar{F}_{other}$ , to give  $\mathcal{M}_o, F_{in}, F_{other}$  (and  $F_{other,+}$  by way of verification).
- 3) In Block1, calculate thanks to (35), the resultant of the reaction wrenches  $F_c$  induced by the contacts.

<sup>2</sup>with the risk, if this is not the case of preventing mobility and, due to the hyper-statism, of producing internal stress resolved by replacing the constraints induced by the internal joints, assumed ideal, by rheological passive laws.

- 4) After a distribution<sup>3</sup> of  $F_c$  at the  $p$  contact points  $C_{i=1,\dots,p}$ , integrate in Block2 the spatial ODE (23) subjected to the distribution of reaction wrenches  $(F_{c,\pm}, \bar{F}_{c_i})$  applied at the contact points, and initialized by  $\mathcal{X}_2(0) = (g_o, \eta_o, \dot{\eta}_o, F_-)$  to calculate the internal wrenches  $\Lambda$ .

## Remarks:

- In the following we do not specify the form of the locomotion kinematics beyond its expression (34), preferring to investigate it, case by case, for particular examples. Let us just say here that the function  $f$  in (34) must be calculated from  $f_1$  of (22) and from considerations related to the way of locomotion studied (particularly based on biological observation) as well as the contact model as introduced in section VI.
- Hyper-redundant manipulators can be considered as a subclass of fully constrained case. In fact here, the reference cross section  $X = 0$  is clamped in a rigid basis enduring an imposed motion (in particular, null) defined by  $\mathcal{X}_1(0) = (g_o, \eta_o, \dot{\eta}_o)(t)$ . In this case, steps 1, 2 and 3 of the above algorithm can be avoided. Indeed, the reference motions require no calculations as they are known by their time laws.
- Note that if  $f$  is linear in  $\dot{\xi}_d$  and independent of  $g_o$ , the kinematic model under the constraints of contacts defines a principal kinematic connection on the principal fiber bundle  $\mathcal{C}_2$ , i.e. a continuous version of the discrete connections studied in the mechanics of non-holonomic systems [30].

## VIII. ILLUSTRATIVE EXAMPLES

We now consider several examples of terrestrial locomotion where the net motions are ruled by kinematic locomotion deduced from the model of contacts summarized in table II.

## A. burrowing worm in 1D

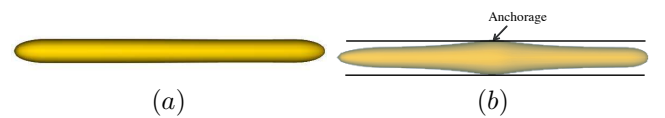


Fig. 6. (a) Initial reference configuration; (b) Deformed configuration

This is a burrowing robot inspired by earthworms. The earthworm is assumed to have a homogenous volumetric mass  $\rho$ . Based on biological knowledge [35], the radial dilation of the cross sections caused by axial compression ensures the worm's anchorage in its surroundings: a tunnel burrowed by prior digestion of the earth in front of the head. Locally, the radial anchorage is achieved by rigid setae which push into the earth radially when the cross section is at maximal dilation (see Fig. 6(b)). The beam model is that of a rod actuated

<sup>3</sup>Univocal if the number of constraints equal the dimension of the fiber, multivocal, if it is higher.



in traction-compression. The forward gait is produced by a backward wave of traction-compression of the form:

$$\Gamma_{dX}(X, t) = 1 + \epsilon \sin(\omega(t - X/c)). \quad (36)$$

The dilation (striction) of the cross sections is controlled by the traction by adding to the Cosserat theory presented earlier the axial volume preservation constraint written as:

$$A(X, t) = A(X, 0)/\Gamma_{dX}(X, t), \quad (37)$$

which is simply derived from:  $A(X, t)dS = A(X, 0)dX$  where  $A(X, t)$  is the area of the cross section  $X$  at the instant  $t$ , while  $dS = \Gamma_{dX}dX$  is the length at current  $t$  of the part of the worm of initial length  $dX$  initially located at  $X$ .

In this scenario, the previous general construction applies by replacing  $G$  (as well as  $\mathfrak{g}$  and  $\mathfrak{g}^*$ ) by  $\mathbb{R}$  identified with the commutative subgroup of translations along the  $x$ -axis (which also coincides with its Lie algebra and its dual). It follows that the adjoint maps disappear from the expressions and we can propose more simply  $g = x$ ,  $g_o = x_o$ ,  $\eta = \dot{x}$ ,  $\xi_d(t) = \Gamma_{dX}$ ,  $\bar{F} = \sum_{i=1}^{i=p} n_{c_i} \delta(X - C_i(t))$ ,  $\Lambda = n$  where  $C_i$  denotes the material abscissas of the  $p$  anchorage points (see Fig. 6(b)) defined at each instant by the condition of the local maximal contraction:

$$C_i(t) \in [0, l], \text{ such that: } \Gamma_{dX}(C_i(t), t) = 1 - \epsilon. \quad (38)$$

With these considerations, the worm's continuous kinematic model takes the form (22) with:

$$\mathcal{X}'_1 = (x', \dot{x}', \ddot{x}')^T = (\Gamma_{dX}(t), \dot{\Gamma}_{dX}(t), \ddot{\Gamma}_{dX}(t))^T, \quad (39)$$

whose solutions are fixed by the anchorage points. In particular, it should be noted that any cross section anchored to the ground by the setae imposes a constraint on the movement in the fiber, identified here to  $\mathbb{R}$ . It follows that the net movements are derived from a kinematic model. Such a model can be simply obtained by imposing that, at any anchorage point  $C_i(t)$ , the velocity of slipping is null, i.e.  $C_i(t)$  represents a sweeping anchorage point. Also, by invoking the contact kinematics (30) with  $C(t) = C_i(t)$ ,  $\eta(C(t)) = \dot{x}(C_i(t))$ ,  $\xi_d(t) = \Gamma_{dX}(t)$ , and  $\eta_c(t) = 0$  (as the obstacles are fixed), then:

$$\dot{x}(C_i(t)) + \Gamma_{dX}(C_i) \dot{C}_i(t) = 0, \quad (40)$$

so that, by taking the velocity of the cross section of the abscissa  $C_i(t)$  from the second line of (39), one obtains:

$$\dot{x}(C_i(t)) = \dot{x}_o + \int_0^{C_i(t)} \dot{\Gamma}_{dX} dX, \quad (41)$$

which can be entered into (40) to give the kinematic model of the earthworm:

$$\dot{x}_o = - \int_0^{C_i(t)} \dot{\Gamma}_{dX} dX - \Gamma_{dX}(C_i) \dot{C}_i(t). \quad (42)$$

Moreover, it is easily shown that, for the law of propagation (36), (42) is independent of the anchorage point considered. In fact,  $\dot{C}_i$  is the speed  $c$  of the traction-compression wave. Thus the locomotion kinematics can be rewritten after time-derivation of (42) with  $i = 1$ :

$$\ddot{x}_o = -\Gamma_{dX}(C_1(t))\dot{c} - \dot{\Gamma}_{dX}(C_1(t))c - \int_0^{C_1(t)} \ddot{\Gamma}_{dX} dX, \quad (43)$$

which enables  $\ddot{x}_o$  to be calculated. After that, it becomes possible, thanks to the external dynamics (35), to calculate the resultant of the reaction forces transmitted by the environment to the worm via the anchorage points:

$$n_c = \sum_{i=1}^{i=p} n_{c_i} = \int_0^l m dX \ddot{x}_o + \int_0^l m \int_0^X \ddot{\Gamma}_{dX} dX dX, \quad (44)$$

where  $m = m(X, t)$  denotes the mass per unit of worm length (and replaces  $\mathcal{M}(X)$ ) while the  $\zeta$  of the general construction is now calculated through space-integration of the continuous model of accelerations (8) initialized by  $\ddot{x}_o = 0$ . Finally, when  $p > 1$  the under-determination of the reaction forces prevents the integration of the internal dynamics. However, if an arbitrary distribution of these forces is assumed such that their resultant verifies (44), for example adopting an equal distribution, i.e.  $n_{c_i} = n_c/p$ , then it becomes possible to integrate (13) which is written here:

$$n' = m(X, t)\ddot{x} - \sum_{i=1}^{i=p} n_{c_i} \delta(X - C_i(t)), \quad (45)$$

with boundary conditions:  $n(0) = n(l) = 0$  if one assumes that the medium presents no force to the front and back of the worm (ingestion and excretion moving the earth matter from in front to behind), and where  $\ddot{x}$  is deduced through space-integration of the kinematic model (39) initialized by:  $(x_o, \dot{x}_o, \ddot{x}_o)$ .

**Numerical results:** For the numerical illustration of the dynamic locomotion of the worm, a forward gait of the type (36) with  $\epsilon = 0.004$  and  $\omega = 2\pi c/\lambda$ , is introduced into the general algorithm applied to the worm. Simulating for 10s, we get the straight line 1D motion of the worm in the  $xy$  plane as shown in Fig. 7. The Fig. 8(a-b) plot the axial position and

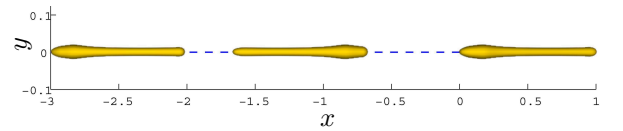


Fig. 7. Worm locomotion in  $xy$  plane

velocity of the worm's head with respect to time, respectively.

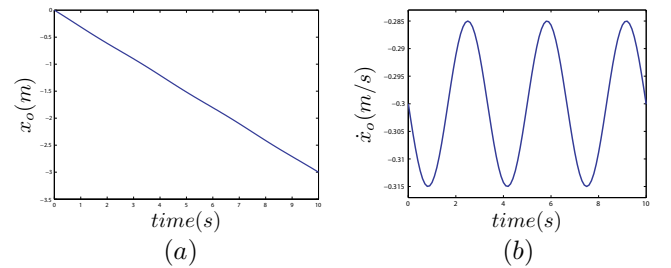


Fig. 8. (a) Time vs head position; (b) Time vs head velocity

The inverse locomotion dynamics and the inverse internal dynamics of the system are solved to get the reaction forces

at the anchorage points and the internal control forces, respectively. By taking the speed  $c = 0.3m/s$  as constant, it is noted that the axial contact force is zero at the anchorage point as shown in Fig. 9(b) at  $X = C$  where no force jump renders the internal force profile discontinuous. This scenario may be compared to that of a wheeled body with constant velocity where the wheels (and hence the body) experiences no external (axial) forces so undergoing a pure inertial motion. Furthermore, by introducing the time dependent speed

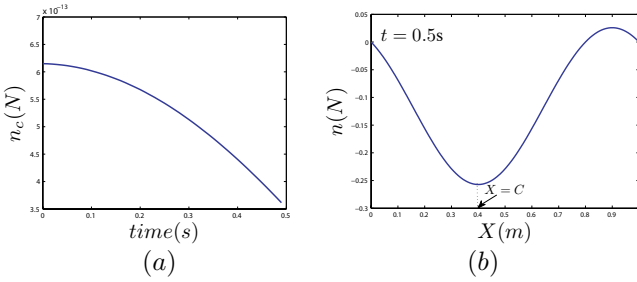


Fig. 9. With constant speed: (a) Contact force; (b) Internal force distribution over the length

$c(t) = at + b$  (with  $a \neq 0$ ), it is noted that, due to the worm accelerations, the axial reaction force ( $n_c$ ) at  $X = C$  is not zero anymore as shown in Fig. 10(a), and hence introduces a jump on the internal control force at  $X = C$ . This appears on Fig. 10(b) which gives the desired internal control force profile applied between cross sections over the whole length.

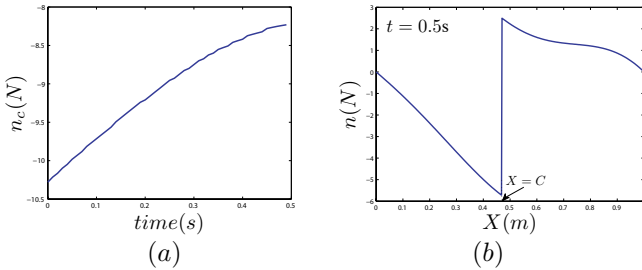


Fig. 10. With variable speed: (a) Contact force; (b) Internal force distribution over the length

### B. Caterpillar (Inchworm) in 2D

We now consider the case of a climbing robot bio-inspired from inchworms. Such an animal can be modeled as a bending actuated beam with one localized clamping in  $C$  alternating from one end to the other at each "step". Such a continuum robot can be modeled by a Kirchhoff planar beam actuated in curvature, i.e. by invoking the previous general construction with  $G = SE(2)$  and  $\xi_d(t) = (1, 0, K_{dZ})^T$  which in this case (planar configuration) is an integrable variable as  $K_{dZ} = \theta'$  where  $\theta$  is the angle that parameterizes the absolute orientation of the cross sections in the plane. Having said that, the locomotion of the caterpillar can be modeled by considering it as a continuous manipulator whose "base" and "terminal" change places at each half-period of its gait. In these conditions, the previous algorithm (with the anchorage point fixed in  $X = 0$ )

can be run again by changing  $X$  into  $l - X$  in the spatial ODE and at each half-period such that  $C = l$ . The gait can be simply defined by the angle  $\theta$  as:

$$\theta(X, t) = \alpha \sin^2(\omega t) \sin\left(\frac{2\pi}{l}(X - l)\right), \quad (46)$$

from which the curvature law is derived:

$$K_{dZ}(X, t) = \alpha \sin^2(\omega t) \left(\frac{2\pi}{l}\right) \cos\left(\frac{2\pi}{l}(X - l)\right). \quad (47)$$

This law ensures that, at each instant:  $\theta(t, X = 0) = \theta(t, X = l) = \theta(t, X = l/2) = 0$  whereas the curvature is minimal at the two ends and maximal at  $X = l/2$ . Finally, the time function as a factor of this internal shape law ensures the periodic relaxation and bending of the robot. Its period is  $\pi/\omega$  and it assures the amplification of the bending over a half-period and its attenuation (down to 0) in the following half-period. Thus, assuming that the caterpillar starts at  $t = 0$  in a stretched position, there will be anchorage at  $X = 0$  at all the intervals  $[2kT, 2kT + T/2]$  and anchorage at  $X = l$  at the intervals  $[2kT + T/2, (2k + 1)T]$ . In these two cases, the external movements are null as they are fixed by the anchorage conditions:  $\mathcal{X}_1(C) = (1, 0, 0)$ . Moreover, the external dynamics enable the reaction at the anchorage point to be calculated. Finally the internal dynamics can be easily integrated (in this case  $\zeta = \eta$ ) to give the internal wrenches.

*Numerical application:* Some numerical results are obtained for caterpillar climbing under gravity by applying the curvature (shape) law (47) as input, with  $\alpha = 1.8$  and  $\omega = 2\pi \cdot 0.25$ . Simulating for 14 sec, we get the motion of the caterpillar in the  $xy$  plane as shown in Fig. 11. The Fig. 12(a-b) plot the axial position and velocity of the caterpillar's head with respect to time, respectively. The inverse locomotion dynamics and the inverse internal dynamics of the system are solved to get the reaction forces at the anchorage points and the internal control torques, respectively. The Fig. 13(a) shows the reaction torque  $c_z(X = 0)$  at head with respect to time. For illustrative purpose, the torque distribution along the length is presented in Fig. 13(b) at  $t = 4.5s$ .

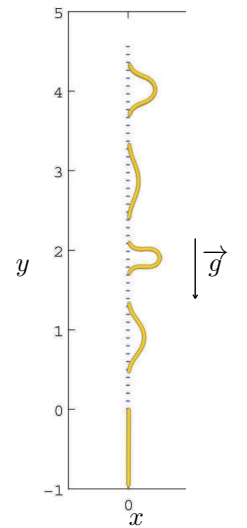


Fig. 11. Caterpillar locomotion in  $xz$  plane

### C. 2D snake in lateral undulation

A snake in lateral undulation is modeled by either a Kirchhoff or a Reissner 2D beam whose discrete counterparts are drawn in Fig. 14(a-b), respectively (the beam cross sections being the continuous infinitesimal counterparts of the axes of the discrete mechanisms). In a first time, we choose the

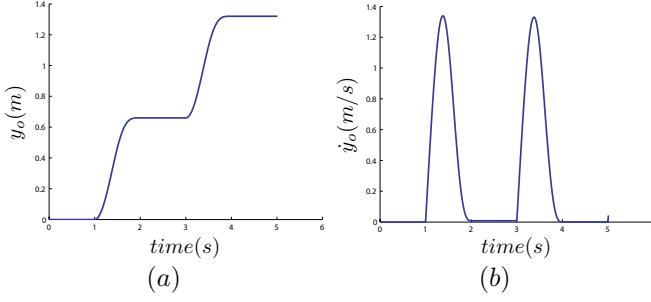


Fig. 12. (a) Time vs head position; (b) Time vs head velocity

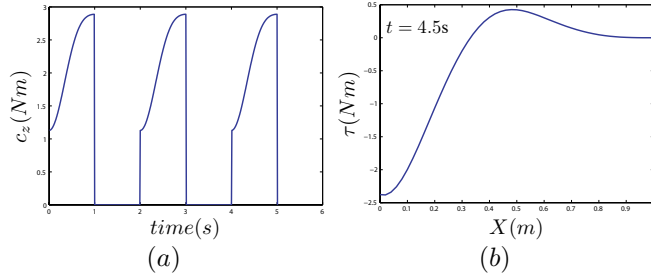


Fig. 13. (a) Reaction torque at head; (b) Internal torque distribution over the length

Kirchhoff-snake kinematic model because it is the simplest and it corresponds to the ACM robots of Hirose [1] whereas the second, as proposed by Ostrowski [36], although more complex, has advantages that we will mention later. In lateral undulation, the snake supports itself laterally in its environment to self propel in an axial direction, i.e. by moving along the length of its backbone. Mathematically, these supports are modeled by non-holonomic constraints preventing the cross sections of the snake to slide laterally. In the case where the contact with the ground is continuously distributed along the body length, there are obviously enough of these constraints for the external movements to be completely fixed by the internal kinematics of the snake according to the kinematic context of section VII. In order to establish this kinematic model, we begin by writing the continuous model of velocities (7) in the case of  $G = SE(2)$  and  $\xi_d(t) = (1, 0, K_{dZ})^T$ . Thus, with  $\eta = (g^{-1}\dot{g})^\vee = (V_X, V_Y, \Omega_Z)^T$ , we have:

$$\begin{pmatrix} V'_X \\ V'_Y \\ \Omega'_Z \end{pmatrix} = \begin{pmatrix} V_Y K_{dZ} \\ \Omega_Z - V_X K_{dZ} \\ \dot{K}_{dZ} \end{pmatrix}. \quad (48)$$

By modeling the contact at each point  $X$  by a CSFS model (section VI-B), the constraints are simply written  $V_Y(X) = 0$ , for  $\forall X \in [0, l]$  (the obstacles being fixed to space). Now, by forcing these (non-sliding) constraints in (48), one obtains the relations which must verify every motion compatible with the supports:

$$\begin{pmatrix} V'_X \\ \Omega_Z \\ \Omega'_Z \end{pmatrix} = \begin{pmatrix} 0 \\ V_X K_{dZ} \\ \dot{K}_{dZ} \end{pmatrix}. \quad (49)$$

From the first line of (49), we see that the axial speed of the snake is constant relative to  $X$  and thus equal to that

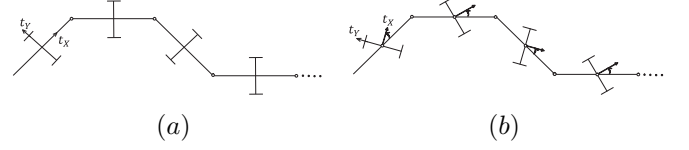


Fig. 14. (a) Kirchhoff-snake; (b) Reissner-snake

of its head, which we will denote more simply  $V_o$  (every function evaluated in  $X = 0$  is indicated with a subscript zero). From the second line, we see that  $\Omega_Z = V_o K_{dZ}$ , i.e. the angular velocity along the snake's backbone is only governed by the forward speed  $V_o$  and the body curvature  $K_{dZ}$ . Next, taking account of lines 1 and 2 in the third, one obtains the fundamental relation:

$$\dot{K}_{dZ} = V_o K'_{dZ}, \quad (50)$$

which must be verified all along the snake so that its mobility (axial propulsion) is assured. Finally, the solutions of (50) take the general form:

$$K_{dZ}(X, t) = f(X + \int_0^t V_o(\tau) d\tau), \quad (51)$$

which corresponds to the propagation of a given curvature profile along the backbone at a generally time-variable speed  $V_o(t)$  (see Fig. 15). It follows that such a choice of the

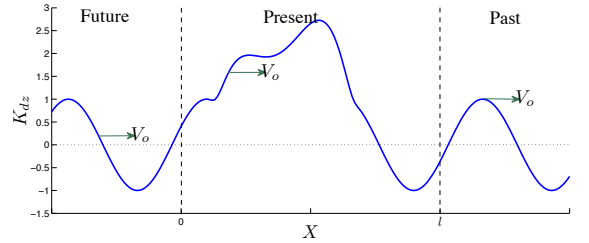


Fig. 15. Curvature profile along the snake's backbone

curvature law ensures the thrust in the direction of  $-t_X(0)$  at the space-constant speed  $V_o(t)$ . Moreover, for all  $X \in [0, l]$ , one can write:

$$\eta_o = \begin{pmatrix} V_o \\ \Omega_o \end{pmatrix} = \begin{pmatrix} 1/K'_{dZ} \\ K_{dZ}/K'_{dZ} \end{pmatrix} (X) \dot{K}_{dZ}(X, t), \quad (52)$$

and, particularly, for  $X = 0$ :

$$\eta_o = \begin{pmatrix} V_o \\ \Omega_o \end{pmatrix} = \begin{pmatrix} 1/K'_o \\ K_o/K'_o \end{pmatrix} \dot{K}_o, \quad (53)$$

which generalizes the connection of the discrete case which encodes the follower-leader kinematics of snakes in lateral undulation. It is worth noting that, just as in the discrete case where the first three axes (starting from the head) fix completely the motion of the head and that of the following links; in the continuous case, the connection (53) involves at most the third derivative of the position field (i.e.  $K'_{dZ}(0) = r'''(0)$ ). In the continuous setting, the principle of the follower-leader kinematics can be stated as follows: once the curvature and its derivative in  $\forall X$  are specified, the velocity of curvature must adapt in each  $X$  so that the cross section  $X - dX$  follows

the cross section  $X$  at the speed  $V_o(t)$ . Thus, every cross section  $X$  reoccupies at  $t^*$  such that  $\int_t^{t^*} V_o d\tau = X$ , the same configuration as that occupied by the head at  $t$ . This explains the impression of lateral stasis and axial movement observed in snakes, which makes their motion resemble a fluid line of a steady flow. In addition, (53) shows that if the axial propulsion is assured by  $\dot{K}_o/K'_o$  it is  $K_o$  that steers the snake in the plane. Thus, we can approach the 2D snake by analogy with another non-holonomic system, more familiar to the robotics engineer: the car-like platform. In this case, the angular steering of the (virtual) front wheels is ensured by  $K_o$  while the thrust produced by the engine is assured by the relation  $\dot{K}_o/K'_o$ .

Turning back to biology, in nature, the curvature along the body of a snake changes according to the choices made by its head, choices that depend on the obstacles that the snake avoid and on which it laterally pushes to propel itself forwards. Consequently such a situation may be represented by a steady profile of curvature moving at the speed  $V_o(t)$  along the body, represented here by the material segment  $[0, l]$  (see Fig. 15 where such a context is illustrated). Finally, for illustration purpose, let us consider the case where  $\dot{V}_o = 0$ , then (50) turns to be the one-dimensional propagation equation whose general solutions are  $K_{dZ}(X, t) = f(t + X/V_o)$ , with  $V_o$  the constant speed of the curvature waves. Then, for environments without obstacles but where the ground plane has good properties to prevent lateral sliding, the law of curvature:

$$K_{dZ}(X, t) = a \cos(\omega(t + X/V_o)) + b \exp\left(-\frac{(t - (t_o + T_o/2) + (X/V_o))^2}{(t - (t_o + T_o/2) + (X/V_o))^2 - (T_o/2)^2}\right), \quad (54)$$

ensures, up to  $t = t_o$ , an axial speed  $-V_o t_X(0)$  of average constant direction, and from  $t = t_o$  generates a turning maneuver of duration  $T_o$ . Next, note that these kinematics are singular when  $K_{dZ} = cte/X$  because, in this case, the conditions of mobility (50) are not verified except in the irrelevant case where the snake has a null motion. To overcome this situation, one can consider the continuous homologue of the discrete kinematics of the Fig. 14(b), i.e. by adding a transverse shearing to the present context. In this case, the kinematics become those of an actuated Reissner planar beam and the continuous model of velocities is rewritten from (48), replacing the first line by the following:

$$V'_X = -K_{dZ} V_X \Gamma_{dY}, \quad (55)$$

so that we now have  $V_X(X) = V_o e^{(-\int_0^X K_{dZ} \Gamma_{dY} dX)}$  and the mobility condition (50) becomes the following:

$$\dot{K}_{dZ} = (K'_{dZ} - K_{dZ}^2 \Gamma_{dY}) V_X, \quad (56)$$

where the presence of the control parameter  $\Gamma_{dY}$  as a factor of  $K_{dZ}$  ensures the mobility of the snake in all cases where  $K_{dZ}(\cdot) \neq 0$ . Thus, we recover that the continuous homologue of the discrete kinematics of the Fig. 14(b) is only singular for the straight configurations as it is only in this case that the internal movements of the odd and even joints cannot produce external movement. Finally, in the case of snakes, the transverse shearing models the movements of the skin and the scales relative to the skeleton whose own movement

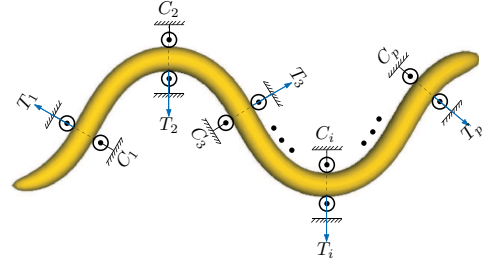


Fig. 16. 2D snake with  $p$  contacts

is modeled by the field of curvature. Also, if a snake finds itself in a perfectly straight configuration, it can remove itself from this singularity by: 1) sliding laterally, 2) leaving the ground. However, if these two possibilities are forbidden (for example, if the snake is made to pass through a straight narrow tube), then only a mode of locomotion like that studied for the earthworm in traction-compression becomes possible.

Finally, as for the net motions computation, taking account of (53), the locomotion kinematics (34) of block0 (Fig. 5) can be written as the system in  $SE(2)$ :

$$\dot{g}_o = g_o \hat{\eta}_o = g_o \begin{pmatrix} 1/K'_o \\ 0 \\ K_o/K'_o \end{pmatrix}^\wedge \dot{K}_o. \quad (57)$$

For the forces, the algorithm integrates at each time-step  $t$ , the system (25) from  $X = 0$  to  $X = l$  initialized in space by  $(g_o(t), \eta_o(t), 0, 0, 0)$ . Then, knowing  $\dot{\eta}_o(t)$  from the time derivative of (53), the algorithm computes in block1 (Fig. 5) via (35) the resultant of the contact wrenches reduced to the head i.e.  $F_c$ . Knowing this resultant, we must formulate a hypothesis for the distribution of the contact forces in order to compute the distribution of the internal forces and torques. For example, assuming that the snake is permanently in contact with the ground via  $p$  supports whose positions are fixed in space as indicated on Fig. 16. Then the load is generally hyper-static (when  $p > 3$ ), and the determination of the lateral contact forces distribution:  $T_{i=1,2,\dots,p}$ , requires the generalized inversion of the under-determined system:

$$F_c = \sum_{i=1}^{i=p} A d_{k(C_i)}^* \begin{pmatrix} 0 \\ T_i \\ 0 \end{pmatrix}, \quad (58)$$

where we recall that  $k(C_i) = g^{-1}(C_i)g_o(t)$ , and we consider the motion while the  $p$  points of contact  $C_{1,2,\dots,p}$  are contained in  $]0, l[$  (see Fig. 16). Once these  $p$  forces are known, the algorithm can integrate in block2 (Fig. 5) the internal dynamics (23) with initial spatial conditions:  $(g_o(t), \eta_o(t), \dot{\eta}_o(t), 0)$  and a distribution of external forces<sup>4</sup>:  $\bar{F} = \sum_{i=1}^p (0, T_i, 0)^T \delta(X - C_i)$ .

**Numerical results:** In case of the 2D snake, an undulatory gait of the type (54) is imposed as input of the algorithm (of section VII). The undulation is provided with  $b \neq 0$  for

<sup>4</sup>This can be achieved by piece-wise integrating the internal dynamics on  $[0, C_1] \cup [C_1, C_2] \cup \dots \cup [C_p, l]$ , using the jump conditions:  $N(C_{i-}) = -T_i + N(C_{i+})$  and  $M(C_{i-}) = M(C_{i+})$  where  $(N^T(C_{i-}), M^T(C_{i-}))^T$  and  $(N^T(C_{i+}), M^T(C_{i+}))^T$  respectively denote the material wrench of internal forces  $\Lambda$  evaluated on the left and the right sides of the cross section  $C_i$ .



certain period of time  $T_o$  which quantifies the amplitude of a turning maneuver in  $SE(2)$ , where  $a = 10$ ,  $\omega = 2\pi V_o/\lambda$  and  $V_o = -0.5m/s$ . Simulating for  $10s$ , the  $2D$  motion of the snake in the  $xy$  plane is shown in Fig. 17. Furthermore, the

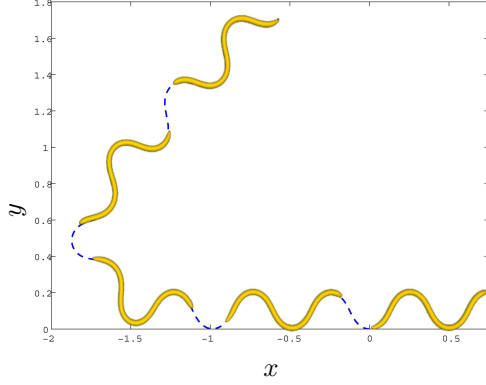


Fig. 17. Snake turning locomotion

locomotion and internal dynamics of the system are solved for  $p = 5$  to obtain the cross sectional reaction wrenches applied at the contact points  $C_1, C_2, \dots, C_5$  (see Fig 16) and the internal control torques, respectively. The Fig. 18(a) plots the reaction force ( $n_y$ ) over the length. The Fig. 18(b) shows the torque distribution over the length of snake at  $t = 2.0s$ .

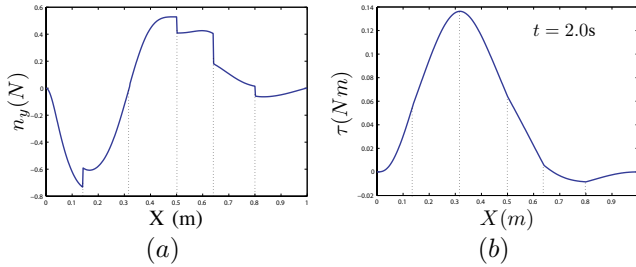


Fig. 18. (a) Contact force ( $n_y$ ) over the length; (b) Internal torque distribution over the length

#### D. 3D snake in lateral undulation

Here we consider only the kinematic aspects of 3D crawling. The 3D snake is a priori modeled by Kirchhoff kinematics with torsion. In this case, we have  $G = SE(3)$  and  $\xi_d = (1, 0, 0, K_{dX}, K_{dY}, K_{dZ})^T$  so that the kinematic model (7) is now written:

$$\begin{pmatrix} V'_X \\ V'_Y \\ V'_Z \\ \Omega'_X \\ \Omega'_Y \\ \Omega'_Z \end{pmatrix} = \begin{pmatrix} V_Y K_{dZ} - K_{dY} V_Z \\ \Omega_Z + K_{dX} V_Z - V_X K_{dZ} \\ -\Omega_Y + K_{dY} V_X - K_{dX} V_Y \\ \dot{K}_{dX} + \Omega_Y K_{dZ} - \Omega_Z K_{dY} \\ \dot{K}_{dY} + \Omega_Z K_{dX} - \Omega_X K_{dZ} \\ \dot{K}_{dZ} + \Omega_X K_{dY} - \Omega_Y K_{dX} \end{pmatrix}. \quad (59)$$

On the basis of this model, we shall first research the 3D homologue of the gaits previously exhibited in 2D. This requires establishing the constraints of non-sliding in 3D, which is simply achieved by proposing that, for every material abscissa

$X$ , the contact is modeled by a cross sectional follower support so that using (32) with  $\Omega_{cX} = V_{cY} = V_{cZ} = 0$ , one has:

$$V_Y(X) = V_Z(X) = 0, \Omega_X(X) = 0, \forall X \in [0, l], \quad (60)$$

which are 3 non-holonomic constraints that must verify each of the cross sections in movement. Next, we introduce these relations into the general kinematic model (59). As a straightforward consequence, the first three equations of (59) allows one to write:

$$V_X = V_o, \Omega_Y = V_o K_{dY}, \Omega_Z = V_o K_{dZ}, \quad (61)$$

where  $V_o$  is again the axial uniform speed along the backbone while the two last of these relations translate the fact that the internal angular velocity of the cross sections is entirely due to the axial movement along a given profile of fixed curvature. Now taking into account the above relations in the fourth equation of (59) in which  $\Omega_X = 0$  is forced, we simply find:

$$\begin{aligned} \dot{K}_{dX} &= \Omega'_X + \Omega_Z K_{dY} - \Omega_Y K_{dZ} \\ &= 0 + V_o (K_{dY} K_{dZ} - K_{dZ} K_{dY}) = 0. \end{aligned} \quad (62)$$

Thus, if we assume that the robot starts (at  $t = 0$ ) from a straight untwisted configuration, one have  $K_{dX} = 0$  all along its length and at any instant of the motion. Introducing this last constraint as well as all the others into the two last relations of (59) allows one to write with (62), the three independent relations on the strain laws:

$$\begin{pmatrix} \dot{K}_{dX} \\ \dot{K}_{dY} \\ \dot{K}_{dZ} \end{pmatrix} = \begin{pmatrix} 0 \\ K'_{dY} V_o \\ K'_{dZ} V_o \end{pmatrix}, \quad (63)$$

where the first of these relations can be ensured by the design (un-twistable kinematics) while the two others are imposed by the curvature control laws. Finally (63) defines the 3D counterpart of the planar mobility condition (50). Continuing in the same way as for the 2D case, we find the 3D external kinematic model in the form of the follower-leader connection:

$$\dot{g}_o = g_o \begin{pmatrix} V_o \\ 0_{3 \times 1} \\ \Omega_{oY} \\ \Omega_{oZ} \end{pmatrix}^{\wedge} = g_o \begin{pmatrix} 1/K'_o \\ 0_{3 \times 1} \\ K_{oY}/K'_o \\ K_{oZ}/K'_o \end{pmatrix}^{\wedge} \dot{K}_o, \quad (64)$$

with  $\dot{K}_o = \|K_d\|'(0)$  et  $K'_o = \|K_d\|'(0)$ .

*Numerical results:* In case of 3D snake, the undulatory motion (54) along with:

$$\begin{aligned} K_{dX}(X, t) &= 0, K_{dY}(X, t) = \\ b_y \exp &\left( -\frac{(t - (t_o + T_o/2) + (X/V_o))^2}{(t - (t_o + T_o/2) + (X/V_o))^2 - (T_o/2)^2} \right), \end{aligned}$$

is given as input to the general algorithm, with  $a = 10$ ,  $\omega = 2\pi V_o/\lambda$ ,  $b_y = 0.5$  and  $V_o = -0.5m/s$ . Simulating for  $10s$ , the 3D motion of the snake in the  $xyz$  space is obtained as shown in Fig. 19.

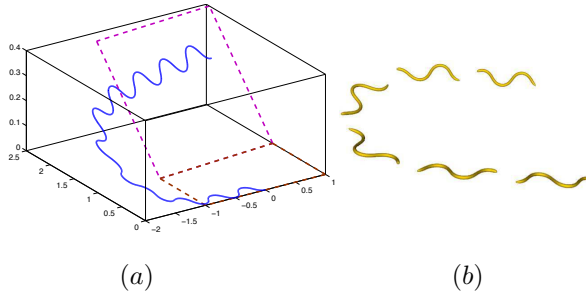


Fig. 19. (a) Head turning locomotion; (b) Snapshots of snake 3D turning locomotion

## IX. GENERAL DISCUSSION AND CONCLUSION

In this article, we have proposed a general abstract framework for modeling continuous style like robots at a macroscopic scale. The solution turns out to be a continuous counterpart of the Newton-Euler dynamics of discrete multibody systems, where the robot is here considered as a strain-actuated Cosserat beam i.e. a serial continuous multi-body system. Once embedded in the framework of locomotion theory on fiber bundles, the approach is exploited to derive an algorithm capable of computing the torques as well as the rigid net motions involved in any locomotion task. The approach as a whole is applied to the case of on ground locomotion where the model of external forces is replaced by the kinematic holonomic and/or nonholonomic constraints of a set of models of contact of practical interest in terrestrial locomotion. It is then applied to several examples inspired by natures. Through these examples, it shows that it can be a useful tool of investigation when it is applied to the analysis of mobility or gait generations of snakes. In the case of earth-worm, the Cosserat assumption of beam cross sections rigidity is removed and replaced by the axial volume preservation constraint. This allows with small efforts to extend the approach and the algorithm to one dimensional hydrostats. The problem of manipulation is illustrated indirectly through the example of the climbing inchworm where at each step of the "walking" the robot is a manipulator clamped into the ground.

Finally, in a second step the question of how applying these results to real designs naturally arises. About this point, the proposed approach being general, the cost to pay for this generality is a certain idealization of the model. This idealization essentially concerns two points: 1°) the model of the body as an internally actuated Cosserat beam. 2°) the model of the contacts between the body and its surroundings. As regards the first point, we today suggest to proceed case by case. For instance, for a specific technology among the numerous designs of snake-like robots today developed [37], [38], one could first ask the starting questions: does the basic Cosserat assumption of rigid cross sections have a physical reality? And also, how this assumption can be adapted to a particular technological principle? As a first answer, let us remark that in the case of designs inspired from vertebrate animals where one can identify lateral rigid elements attached to a body line axially articulated and mimicking the backbone, the Cosserat model is more and more well adapted as the number of vertebrae increases (big snakes like pythons can have more than several hundred). In a design more inspired

from hyper-redundant arthropods, the rigid segments can also be considered as being the cross sections of their macro-continuous model. Finally, for robots inspired from hydrostats, although the application of the approach seems less natural since these animals do not contain any rigid element in their principle, we saw in the article, how we could release the Cosserat basic assumption of rigid cross sections in order to adapt the model to a simplified version of one dimensional hydrostats. Furthermore, some groups today exploring new designs in soft robotics have chosen to mimic hydrostats as a set of rigid cross-sections interconnected and through actuated cables and refer explicitly to the Cosserat model as a source of inspiration for their design [7]. Finally, as elasticity plays an important role in continuous robots, the body model proposed in the article could be improved in this sense. About the second point (the model of the contacts), let us remind that in the case of snake-like robots, we have modeled the contacts through bi-lateral annular joints introducing a null axial friction (along the vertebral axis) as well as an infinite lateral friction force (perpendicular to the vertebral axis). In spite of its ideal character, such a model is not so far from what one can observe on real snakes. Indeed, the scales of the snakes give to their skin a strong frictional anisotropy, the axial friction being far lower than its lateral counterpart. In our case, we pushed this tendency to its ideal asymptotic limit, and also replaced the usual unilateral contacts by bi-lateral constraints. This second simplification, which can be released in future, requires a further discussion on the feasibility of a motion. Indeed, once the net motions known by solving the external kinematics, one has to check whether the real contacts can generate the desired external wrench? Technically, the answer to this question depends on the solutions of a linear system of the form<sup>5</sup> (58). In particular, if the joints are in reality unilateral contacts (as this is the case of obstacle-aided locomotion [37]), the reaction forces solutions of (58) should have to keep a given sign all along the motion. At last, once such a loading has been found, so validating the model of contacts, one has to check whether the actuators can supply the desired motions under such a loading. In order to address this last problem, one can use the inverse dynamics of control torques. Now, coming back to nature, for a snake moving in a tree for instance, the animal permanently exploits the redundancy of (58) in order to satisfy supplementary more sophisticated conditions as maximizing the adherence while minimizing the consumed energy... Among the degrees of freedom of these solutions that the snakes exploit, they can change the configuration of the contacts with time and play with the internal control forces which do not produce any net motion. Finally, if we seek a design of snake-like robot ideally adapted to our model of robot and contacts, starting from [39], this would be a multi-body system with a very high number of very small length links connected through universal joints. Each of these links would be equipped with many wheels aligned along its greater length and placed radially on the links, so bio-mimicking the scales of a 3D snake (see Fig. 20). Finally, as the number of the links increases, it becomes

<sup>5</sup>In fact its 3D generalization.



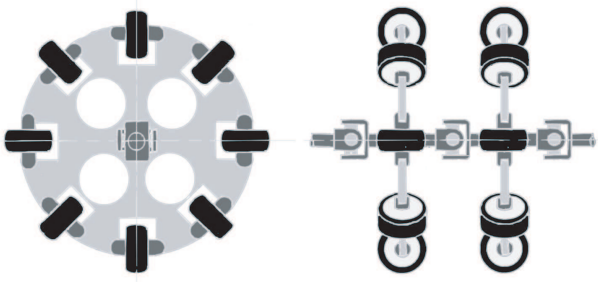


Fig. 20. Proposed design of a 3D snake

more and more relevant to approximate the robot behavior with continuous models [13], [40]. In this case, the Newton-Euler formulation (as proposed in the article) allows solving the dynamics without re-parameterizing the model through a set of generalized coordinates (finite elements or assumed modes...), as it is required by the Lagrangian approach of the same problem. From a pure computational aspect, when the number of d.o.f. dramatically increases, the recursive formulations of chained systems dynamics, as that of Newton-Euler, become more and more efficient since they lead to  $O(n)$  algorithms with  $n$  the number of links. Furthermore, due to their implicit character, the Newton-Euler algorithms are simple to program on a computer. In the continuous case here presented, these recursive computations are replaced by o.d.e.'s which are solved through standard adaptive step numerical integrators allowing to increase further the computational efficiency. Finally, these virtues have been exploited in the presented article to implement simulators, which are faster than real time for all the reported examples.

#### APPENDIX A NOTATIONS

This appendix provides some basic insights of the notations of geometric mechanics [31]. The element  $g \in SE(3)$  is a  $4 \times 4$  homogeneous transformation matrix that defines the mapping between two frames:

$$g = \begin{pmatrix} R & r \\ 0 & 1 \end{pmatrix}. \quad (65)$$

$Ad_g$  is a  $6 \times 6$  matrix that once applied to a vector or twist changes it from one frame to another frame separated by transformation element  $g$ , where:

$$Ad_g = \begin{pmatrix} R & -R \hat{r} \\ 0 & R \end{pmatrix}. \quad (66)$$

For a given  $\eta = (V^T, \Omega^T)^T \in \mathbb{R}^6$ ,  $ad_\eta$  is a  $6 \times 6$  matrix that once applied to a vector (or twist), changes it from one frame to another frame separated by the infinitesimal transformation  $(1 + \hat{\eta})$ :

$$ad_\eta = \begin{pmatrix} \hat{\Omega} & \hat{V} \\ 0 & \hat{\Omega} \end{pmatrix}. \quad (67)$$

Passing to dual,  $Ad_g^*$  and  $ad_\eta^*$  define the  $6 \times 6$  matrices that change any dual vector (or wrench) from one frame to another frame separated by  $g^T$  and  $(1 + \hat{\eta})^T$ , respectively. Where,  $Ad_g^* = Ad_g^T$  and  $ad_\eta^* = ad_\eta^T$ .

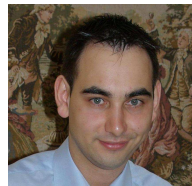
#### REFERENCES

- [1] S. Hirose, *Biologically inspired robots: Snake-like locomotors and manipulators*. Oxford: Oxford Univ. Press, 1993.
- [2] F. Boyer, M. Porez, and W. Khalil, "Macro-continuous computed torque algorithm for a three-dimensional eel-like robot," *IEEE Trans. Robot.*, vol. 22, pp. 763–775, Aug. 2006.
- [3] M. W. Hannan and I. D. Walker, "Kinematics and the implementation of an elephant's trunk manipulator and other continuum style robots," *J. Robot. Syst.*, vol. 20, no. 2, pp. 45–63, 2003.
- [4] H. Takanobu, T. Tandai, and H. Miura, "Multi-dof flexible robot base on tongue," in *Proc. IEEE Int. Conf. Robot. Autom.*, vol. 3, pp. 2673–2678, 2004.
- [5] K. Bose and A. Dorfmann, "Computational aspects of a pseudo-elastic constitutive model for muscle properties in a soft-bodied arthropod," *International Journal of Non-Linear Mechanics*, vol. 44, no. 1, pp. 42–50, 2009.
- [6] B. Kim, M. G. Lee, Y. P. Lee, Y. Kim, and G. Lee, "An earthworm-like micro robot using shape memory alloy actuator," *Sensors and Actuators A: Physical*, vol. 125, no. 2, pp. 429–437, 2006.
- [7] C. Laschi, B. Mazzolai, V. Mattoli, M. Cianchetti, and P. Dario, "Design of a biomimetic robotic octopus arm," *Bioinspiration & Biomimetics*, vol. 4, no. 1, p. 015006 (8pp), 2009.
- [8] D. Trivedi, C. D. Rahn, W. M. Kier, and I. D. Walker, "Soft robotics: Biological inspiration, state of the art, and future research," *Applied Bionics and Biomechanics*, vol. 5, no. 3, pp. 99–117, 2008.
- [9] G. S. Chirikjian and J. W. Burdick, "A hyper-redundant manipulator," *IEEE Robot. Automat. Mag.*, pp. 22–29, Dec. 1994.
- [10] J. W. Burdick, J. Radford, and G. S. Chirikjian, "A 'sidewinding' locomotion gait for hyper-redundant robots," in *Proc. IEEE Int. Conf. Robot. Autom.*, pp. 101–106, May. 1993.
- [11] S. Neppalli, M. A. Csencsits, B. A. Jones, and I. D. Walker, "A geometrical approach to inverse kinematics for continuum manipulators," in *Proc. IEEE/RSJ Int. Conf. Intell. Robots Syst.*, pp. 3565–3570, Sept. 2008.
- [12] B. A. Jones and I. D. Walker, "Kinematics for multisection continuum robots," *IEEE Trans. Robot.*, vol. 22, no. 1, pp. 43–55, 2006.
- [13] G. S. Chirikjian and J. W. Burdick, "The kinematics of hyper-redundant robot locomotion," *IEEE Trans. Robot. Autom.*, vol. 11, pp. 781–793, Dec. 1995.
- [14] I. A. Gravagne, C. D. Rahn, and I. D. Walker, "Good vibrations: a vibration damping setpoint controller for continuum robots," in *Proc. IEEE Int. Conf. Robot. Autom.*, vol. 4, pp. 3877–3884, 2001.
- [15] H. Mochiyama and T. Suzuki, "Kinematics and dynamics of a cable-like hyper-flexible manipulator," in *Proc. IEEE Int. Conf. Robot. Autom.*, vol. 3, pp. 3672–3677, 2003.
- [16] E. Tatlicioglu, I. D. Walker, and D. M. Dawson, "Dynamic modelling for planar extensible continuum robot manipulators," in *Proc. IEEE Int. Conf. Robot. Autom.*, pp. 1357–1362, Apr. 2007.
- [17] W. Khalil, G. Gallot, O. Ibrahim, and F. Boyer, "Dynamic modeling of a 3-D serial eel-like robot," in *Proc. IEEE Int. Conf. Robot. Autom.*, pp. 1270–1275, Apr. 2005.
- [18] F. Matsuno and H. Sato, "Trajectory tracking control of snake robots based on dynamic model," in *Proc. IEEE Int. Conf. Robot. Autom.*, pp. 3029–3034, Apr. 2005.
- [19] G. S. Chirikjian, "A continuum approach to hyper-redundant manipulator dynamics," in *Proc. IEEE/RSJ Int. Conf. Intell. Robots Syst.*, vol. 2, pp. 1059–1066 vol.2, Jul. 1993.
- [20] R. L. Hatton and H. Choset, "Generating gaits for snake robots by annealed chain fitting and keyframe wave extraction," in *Proc. IEEE/RSJ Int. Conf. Intell. Robots Syst.*, IROS'09, pp. 840–845, 2009.
- [21] J. C. Simo and L. Vu-Quoc, "A three-dimensional finite-strain rod model. part II: Computational aspects," *Comp. Meth. Appl. Mech. Eng.*, vol. 58, pp. 79–116, 1986.
- [22] J. C. Simo, "A finite strain beam formulation. the three-dimensional dynamic problem. part I: Formulation and optimal parametrization," *Comp. Meth. Appl. Mech. Eng.*, vol. 72, pp. 267–304, 1989.
- [23] R. J. Webster, J. S. Kim, N. J. Cowan, G. S. Chirikjian, and A. M. Okamura, "Nonholonomic modeling of needle steering," *Int. J. Rob. Res.*, vol. 25, no. 5-6, pp. 509–525, 2006.

- [24] D. C. Rucker, B. A. Jones, and R. J. Webster, "A geometrically exact model for externally loaded concentric-tube continuum robots," *IEEE Trans. Robot.*, vol. 26, pp. 769–780, Oct. 2010.
- [25] D. Trivedi, A. Lotfi, and C. D. Rahn, "Geometrically exact models for soft robotic manipulators," *IEEE Trans. Robot.*, vol. 24, pp. 773–780, Aug. 2008.
- [26] M. D. Grissom, V. Chitrakaran, D. Dienno, M. Csencits, M. Pritts, B. Jones, W. McMahan, D. Dawson, C. Rahn, and I. Walker, "Design and experimental testing of the OctArm soft robot manipulator," in *Society of Photo-Optical Instrumentation Engineers (SPIE) Conference Series*, vol. 6230 of *Presented at the Society of Photo-Optical Instrumentation Engineers (SPIE) Conference*, June 2006.
- [27] E. Cosserat and F. Cosserat, *Théorie des corps déformables*. Hermann, Paris, 1909.
- [28] J. E. Marsden, R. Montgomery, and T. S. Ratiu, "Reduction, symmetry, and phases in mechanics," *Memoire AMS*, vol. 436, 1990.
- [29] F. Boyer and S. Ali, "Recursive inverse dynamics of mobile multibody systems with joints and wheels," *IEEE Trans. Robot.*, vol. 27, pp. 215 – 228, April 2011.
- [30] A. M. Bloch, *Nonholonomic Mechanics and Control*. New York: Springer-Verlag, 2007.
- [31] V. I. Arnold, *Mathematical Methods in Classical Mechanics*. New-York: Springer-Verlag, 1988.
- [32] D. C. Rucker, R. J. Webster, G. S. Chirikjian, and N. J. Cowan, "Equilibrium conformations of concentric-tube continuum robots," *Int. J. Rob. Res.*, vol. 29, no. 10, pp. 1263–1280, 2010.
- [33] F. Boyer, M. Porez, and A. Leroyer, "Poincaré- $\frac{1}{2}$ -cosserat equations for the lighthill three-dimensional large amplitude elongated body theory: Application to robotics," *Journal of Nonlinear Science*, vol. 20, pp. 47–79, 2010.
- [34] F. Boyer, M. Porez, A. Leroyer, and M. Visonneau, "Fast dynamics of an eel-like robot-comparisons with navier-stokes simulations," *IEEE Trans. Robot.*, vol. 24, pp. 1274–1288, Dec. 2008.
- [35] E. Ruppert and R. Barnes, *Invertebrate Zoology*. Fort Worth, TX: Saunders College Publishers, 1994.
- [36] J. P. Ostrowski and J. W. Burdick, "Gait kinematics for a serpentine robot," in *Proc. IEEE Int. Conf. Robot. Autom.*, pp. 1294–1299, 1996.
- [37] P. Liljebäck, K. Y. Pettersen, O. Stavdahl, and J. T. Gravdahl, "Experimental investigation of obstacle-aided locomotion with a snake robot," *Robotics, IEEE Transactions on*, vol. 27, pp. 792 –800, aug. 2011.
- [38] A. A. Traneth, K. Y. Pettersen, and P. Liljebäck, "A survey on snake robot modeling and locomotion," *Robotica*, vol. 27, no. 07, pp. 999–1015, 2009.
- [39] H. Yamada, S. Chigisaki, M. Mori, K. Takita, K. Ogami, and S. Hirose, "Development of amphibious snake-like robot acm-r5," in *Proc. 36th Int. Symposium on Robotics*, 2005.
- [40] G. S. Chirikjian, "Hyper-redundant manipulator dynamics: A continuum approach," *Advanced Robotics*, vol. 9, no. 3, pp. 217–243, 1994.



**Shaukat ALI** received a B.Sc. (Hons.) degree in Mechanical Engineering from the NWFP University of Engineering and Technology Peshawar, Peshawar, Pakistan in 2004 and a Master of Research degree in Robotics from the Ecole Centrale Nantes, Nantes, France in 2008. He is currently working toward a Ph.D. degree at the Ecole des Mines de Nantes in the Institut de Recherche en Communication et Cybernétique de Nantes (IRCCyN) on the dynamic modeling of multibody systems.



**Mathieu Porez** born in France in 1980. He obtained the University Degree of Technology in Mechanics and Industrial Engineering from the Université de Rennes (France) in 2000. He obtained the Master of Technology in Material forming and the Master of Science in Materials, Mechanical engineering and Fluid Mechanics from Université de Lorient (France) in 2003. He obtained the Ph.D of Robotics from the Université de Nantes in 2007. Since February 2009, he has been PostDoc at the BioRob Laboratory of the EPFL (Switzerland). His research topics include

Bio-Robotics and Fluid Mechanics.



**Frédéric BOYER** was born in France in 1967. He received a Diploma in Mechanical Engineering from the Institut Nationale Polytechnique de Grenoble, Grenoble, France in 1991, a Master of Research degree in Mechanics from the University of Grenoble in 1991 and a Ph.D. degree in Robotics from the University of Paris VI, Paris, France in 1994.

He is currently a Professor at the Department of Automatic Control, Ecole des Mines de Nantes, Nantes, France where he works with the Robotics Team, Institut de Recherche en Communication et

Cybernétique de Nantes (IRCCyN). His current research interests include structural dynamics, geometric mechanics, and bio-robotics. Prof. Boyer was awarded the Monpetit prize of the Academy of Science of Paris in 2007 for the whole of his work in Dynamics.